Eur Biophys J 21, 155–161 (1992)

European Biophysics Journal

Structural organization of guanosine derivatives in dilute solutions: small angle neutron scattering analysis

Flavio Carsughi*, Monica Ceretti, and Paolo Mariani**

Istituto di Scienze Fisiche, Facoltà di Medicina e Chirurgia, Università di Ancona, via Ranieri Monte D'Ago, I-60131 Ancona, Italy

Received January 3, 1992/Accepted March 16, 1992

Abstract. Guanosine derivatives, dissolved in water, can form cholesteric and hexagonal mesophases. The common structural unit is a chiral rod-shaped aggregate consisting of a stack of Hoogsten-bonded guanosine tetrameric disks. In order to elucidate the self-association process, we decided to investigate, by small-angle neutron scattering, the structural properties of d(pG), d(GpG), d(GpGpG), d(GpGpGpG) and d(GpGpGpGpGpG) derivatives in very dilute solutions. Under our experimental conditions only d(pG) seems not to form detectable particles. On the other hand, the results for the other derivatives indicate that cylindrical aggregates, having a 10 Å cross-section gyration radius and a length of about 70 Å, exist in the isotropic phase. According to the structure of the hexagonal and cholesteric phases, we fitted the experimental data by using a model of rod-shaped aggregates formed by stacking about 18 to 20 guanosine tetramers. Moreover, from the measurement of the concentration of scattering particles, we deduced that guanosine derivatives are only partially aggregated, depending on their ability to form mesophases.

Key words: SANS – Lyotropic phases – Guanosines – Structural organization

Introduction

The peculiar ability of "stick" guanosine and some of its derivatives to self-associate into stable structures has been known for a long time (see for example Gellert et al. 1962; Iball et al. 1963; Zimmermann 1976; Saenger 1984). This special feature has been suggested to mediate the pairing, in a parallel fashion, of the four homologous chromatids during meiosis and the dimerization of the telomeric ends of chromosomes (Sundquist and Klug 1989; Jin et al. 1990), and seems to have a prebiotic significance in the origin of the genetic code (Saenger 1984).

In recent papers (Spada et al. 1988; Mariani et al. 1989), the structure of the mesophases that aqueous solutions of the dinucleoside phosphate, 2′-deoxyguanylyl-(3′-5′)-2′-deoxy guanosine d(GpG) (G2), may exhibit, has been described; in particular, the sodium salt of G2 forms cholesteric and hexagonal mesophases as the water content decreases. On the basis of X-ray diffraction and optical microscopy experiments (Mariani et al. 1989), it has been suggested that these liquid crystalline phases consist of rod-shaped chiral aggregates with negative diamagnetic anisotropy. Each rod appears to consist of a stacked array of planar tetramers, formed by Hoogsteen-bonded guanosine moieties (Hoogsten 1959; Saenger 1984), at a typical distance of about 3.3 Å. At high dilution, an isotropic solution is observed; at higher concentration, the four-stranded chiral cylinders give rise to a cholesteric mesophase, characterised by a weak correlation between the rods. By further increasing the concentration, a hexagonal mesophase is finally obtained: in such a structure the rods are arranged in parallel and in a highly ordered array.

Other guanosine derivatives have been also investigated (Spada et al. 1991). In particular, it has been shown that the nucleoside 2′-deoxyguanosine-5′-monophosphate d(pG) (G1), the "trimer" d(GpGpG) (G3), the "tetramer" d(GpGpGpG) (G4) and the "hexamer" d(GpGpGpGpGpG) (G6) also form cholesteric and hexagonal phases. While the overall structures of the four-stranded columnar aggregates appear to be similar to each other and to that of G2, some differences have been demonstrated (Spada et al. 1991). The handness and pitches of the cholesteric phases, as well as the critical concentrations at which phase transitions occur, seem in fact to follow a definite pattern, in relation to the negative charge-guanine units *ratio*, i.e. to the different balance between covalent and non-covalent bonds holding together the oligodeoxyguanilates in the aggregates. From

* *Present address:* Institut für Festkörperforschung, Forschungszentrum Julich, FRG

** *Present address:* Laboratoire Léon Brillouin (Laboratoire Commun CEA-CNRS), CEN Saclay, F-91191 Gif-sur-Yvette Cedex, France

Correspondence to. P Mariani

the analysis of the low angle X-ray diffraction profiles, structural information has been obtained: in particular, for all samples and independent of the water concentration, the rod diameter has been found to be about 26 Å (Spada et al. 1991).

To study how guanosine moieties interact to give rise to the disks and to the columnar aggregates, we decided to investigate the more hydrated region of the phase diagrams. We describe here a small-angle neutron scattering study of the isotropic phase of the G1, G2, G3, G4 and G6 derivatives. The results, which provide information about the number, form and dimensions of the scattering particles, seem to indicate that discrete four-stranded aggregates still exist in the isotropic solution. It is important to point out that, under our experimental conditions, only a fraction of the G2, G3, G4 and G6 molecules appear to be arranged in the rod form, while the G1 derivative seems not to aggregate at all.

Materials and methods

The guanosine derivatives investigated were synthesised according the procedure described by Spada et al. (1991). An analysis of the textures was performed as a function of water concentration by using an optical polarizing microscope, and this confirmed the phase sequence previously determined (Spada et al. 1991). The Isotropic (I) to Cholesteric (Ch) and the Cholesteric (Ch) to Hexagonal (H) phase transition concentrations C, espressed in weight of solute (grams percent), are the following (in water, at 20 °C):

G1:	I	30% Ch	40% H
G2:	I	2,5%Ch	18% H
G3:	I	8% Ch	25% H
G4:	I	13% Ch	35% H
G6:	I	19% Ch	35% H

The small angle neutron scattering (SANS) experiments were carried out at the Laboratoire Leon Brillouin (Saclay, France) using the small-angle diffractometer PAXE, which is situated on a cold neutron guide of the Orphée reactor. The samples were measured at about 20 °C in 2 mm thick quartz cells. The neutron wavelength used was $\lambda = 5$ Å and the sample-detector distance was 2 m, which allows one to investigate a scattering vector Q range between about 0.3×10^{-2} and 0.3 $Å^{-1}$, where the scattering vector Q is defined as $(4\pi \sin\theta)/\lambda$ and 2θ is the full scattering angle.

In order to obtain good statistics, a typical run time of 8 hours was chosen. The raw data were corrected for electronic noise and sample holder signal by measuring a cadmium sample (strong neutron absorber) and an empty quartz cell, respectively. Since the samples scatter neutrons in an isotropic way, the data were radially averaged to improve statistics.

The calibration of the SANS intensities in absolute units allows the determination of quantitative information for the studied system. In the present case, the scattered intensities were calculated in absolute units (cm^{-1}) by comparing their values with those obtained from a 1 mm thick water sample, which has a known macroscopic cross section ($d\Sigma^w/d\Omega$) given by (Jacrot 1976):

$$(d\Sigma^w/d\Omega) = g(\lambda)(1 - T^w)/(4\pi T^w D^w) \quad (1)$$

where T^w is the water transmission factor, D^w the thickness of the water sample and $g(\lambda)$ a correction factor which takes into account inelastic effects and multiple scattering events. At the wavelength used the correction factor is 1.27 (R. Oberthur, private communication).

The incoherent scattering cross section of a 1 mm thickness of water at a 5 Å neutron wavelength is about 0.8 cm^{-1}. Figure 1 shows that in our experiments the SANS signal does not exceed 0.1 cm^{-1}. Taking into account the fact that the neutron contrast factor is different if normal or heavy water is used as solvent, the contrast is about 2.6 times larger in the case of normal water. This is not enough to produce a coherent SANS signal higher than the incoherent background; therefore, the derivatives were dissolved in D_2O. The concentration was 10 mg/ml (i.e. $C = 1\%$). In the case of G1, G2 and G3 derivatives, samples with a 15 mg/ml (i.e. $C = 1.5\%$) concentration were also investigated. The use of these low concentrations avoided undesired interference effects from the scattered neutrons (Abis et al. 1990).

Concerning the solvent, two important points must be noted. First, to calculate the mean particle scattering length (see below), we assume that all the labile hydrogen atoms in the guanosine molecule exchange with the solvent as observed for polynucleotide derivatives (Jacrot and Zaccai 1981). Second, we discuss a possible relationship between the present data and the concentration of the isotropic to cholestric phase transition, which depends on the phase diagram in D_2O. In fact, it is well known that interactions (and then aggregation phenomena) are different in normal and heavy water; in particular, D_2O stabilizes hydrophobic interactions, and in our case this could favour the guanosine self-aggregation process. However, an extended analysis of this type lies outside the aim of the paper, so that we have limited ourselves to verifying by optical polarized microscopy that all the samples investigated were in the isotropic phase. The isotropic to cholesteric phase transition concentration in D_2O was estimated approximately in the case of G1 and G3 derivatives: at 20 °C, their phase diagrams appear insensitive to the use of heavy water as solvent.

Data analysis

In the case of a two phase model with identical scattering centres and random orientation, the coherent macroscopic differential cross section is related to the scattering center parameters by

$$d\Sigma/d\Omega\,(Q) = N\,(\Sigma b - \varrho_S V)^2\,|F(Q)|^2 \quad (2)$$

where N is the number of scattering particles per unit volume, Σb the sum of the scattering length of all the nuclei of the whole scattering particles, ϱ_S the scattering length density of the solvent, V the scattering particle volume and $|F(Q)|^2$ the squared averaged form factor,

which depends on the size and shape of the scattering particles.

Owing to the mathematical properties, at low Q the form factor can be approximated by the so-called Guinier law (Guinier and Fournet 1955; Kratky 1983; Chen and Lin 1987):

$$d\Sigma/d\Omega(Q) \cong d\Sigma/d\Omega(0) \exp(-Q^2 R_g^2/3) \quad (3)$$

where R_g is the gyration radius, defined by:

$$R_g^2 = \Sigma_j((\varrho(r_j) - \varrho_S) V_j r_j^2)/\Sigma_j((\varrho(r_j) - \varrho_S)(V_j). \quad (4)$$

$d\Sigma/d\Omega(0)$ is the coherent intensity scattered at $Q = 0$, which, considering that $F(0) = 1$, is defined by

$$d\Sigma/d\Omega(0) = N(\Sigma b - \varrho_S V)^2. \quad (5)$$

Because of the impossibility of discriminating the SANS signal from the primary beam at low Q and from the background at large Q, a measurement can only investigate over a finite Q range. If the Guinier law is satisfied ($Q R_g < 1.0$), the gyration radius R_g and the $d\Sigma/d\Omega(0)$ value can be obtained by performing a linear fit of the experimental SANS data in the Guinier plot, ln ($d\Sigma/d\Omega(Q)$ vs. Q^2.

Likewise, in the case of rod-like particles at low Q, (2) becomes:

$$d\Sigma/d\Omega(Q) Q \cong (d\Sigma/d\Omega(Q) Q)_{Q \to 0} \exp(-Q^2 R_c^2/2), \quad (6)$$

where $(d\Sigma/d\Omega(Q) Q)_{Q \to 0}$ is the cross-sectional intensity scattered at $Q = 0$ and R_c the gyration radius of the cross section of the scattering particle (Kratky 1983; Chen and Lin 1987); such values can be determined in a similar way to that shown above.

Moreover, a simple relation between R_g and R_c allows the determination of the length of the longest axis L of the scattering particle (Kratky 1983; see also Kratky and Laggner 1987):

$$L^2 = 12(R_g^2 - R_c^2). \quad (7)$$

The combination of $d\Sigma/d\Omega(0)$ (see (3)) and $(d\Sigma/d\Omega(Q) Q)_{Q \to 0}$ (see (6)) values also leads to the length of the same axis of the cylindrical particle (Perkins et al. 1986):

$$L = (\pi d\Sigma/d\Omega(0))/(d\Sigma/d\Omega(Q) Q)_{Q \to 0} \quad (8)$$

Results

SANS cross sections were measured from D_2O solutions of G1, G2, G3, G4 and G6 derivatives at a fixed concentration of 1% w/w and in the case of G1, G2 and G3 also at a concentration of 1.5% w/w. As reported above, D_2O was used as solvent, in order to reduce the incoherent background and to obtain a better signal-to-noise ratio. Moreover, low concentrations were selected in order to avoid undesired interference effects (Abis et al. 1990). In fact, in very dense systems, the interparticle distances are small enough to resolve, in the investigated domain of the reciprocal space, the interparticle structure function. In contrast, in dilute systems, the interference effects give an appreciable contribution to the SANS signal only at very low Q values, which lie outside the investigated Q range.

In Fig. 1 we report the calibrated neutron scattering intensities observed in the case of samples with concentration equal to 1% w/w. It is evident that, at this concentration, the G1 derivative does not aggregate in solution, as its signal is characterized by a flat background, typical of incoherent scattering. In contrast, the other derivatives show SANS signals. The Guinier plot, ln ($d\Sigma/d\Omega(Q)$) vs. Q^2, for the G3 sample is reported in the lower frame of Fig. 2, together with the linear behaviour up to a $Q R_g \approx 1$. In Table 1, the radii of gyration (R_g) and the SANS cross sections at zero angle ($d\Sigma/d\Omega(0)$) determined from the Guinier plots for all the investigated samples are reported: it is interesting to note that the different derivatives show an approximately constant gyration radius of about 20 Å. In the case of the experiments performed at C = 1.5%, the flat signal observed in the case of the G1 sample confirms that no scattering particles are detectable in the investigated Q-range. On the other hand, the G2 and G3 derivatives show scattering curves qualitatively very similar to those observed at the higher dilution; however, the SANS cross sections at zero angle and the gyration radii are larger than those found at the lower concentration (see Table 1).

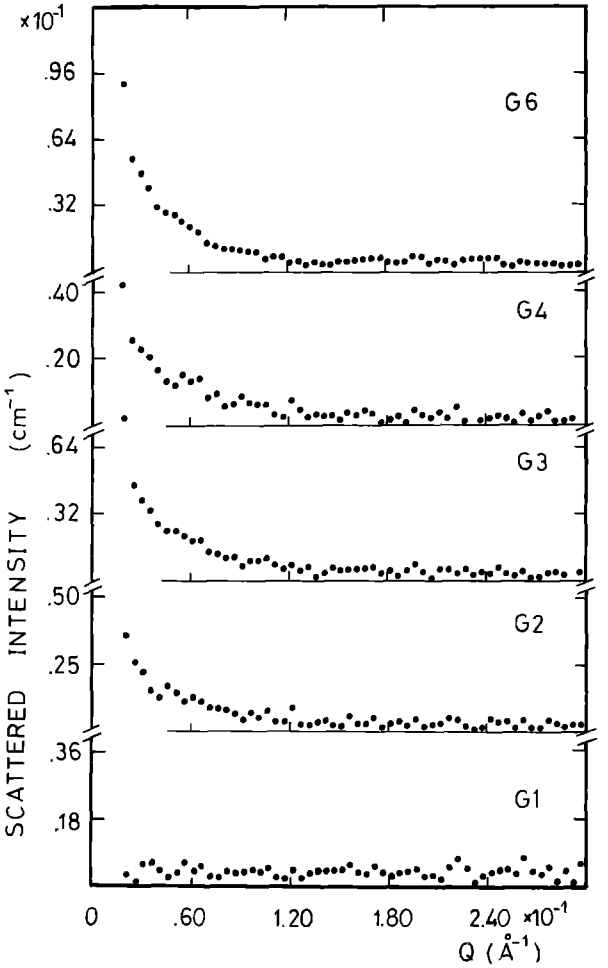

Fig. 1. Neutron scattering intensity profiles for the series of guanosine derivatives investigated ($C = 1\%$). Data are shown on an absolute scale

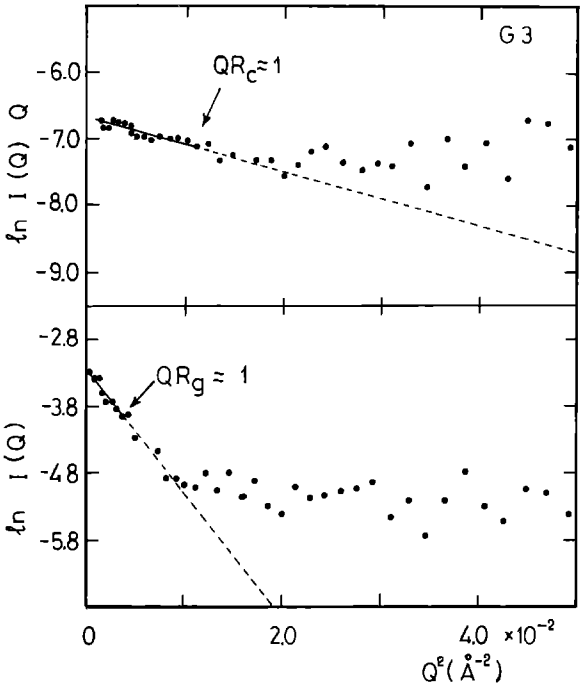

Fig. 2. Representative Guinier analysis of the scattering curve relative to the G3 derivative with $C = 1\%$. Top diagram: Cross-section Guinier plot $\ln(d\Sigma/d\Omega(Q)Q)$ vs. Q^2. Bottom diagram: Guinier plot $\ln(d\Sigma/d\Omega(Q))$ vs. Q^2. The straight lines correspond to the best fit through the experimental points for which the Guinier law is satisfied

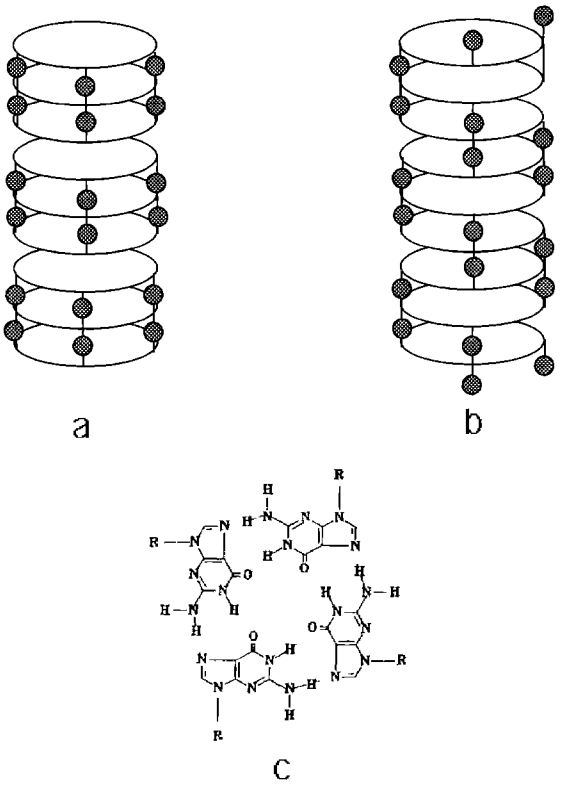

Fig 3a–c. A sketch of the possible models for the rod structure in the case of the G3 derivative: **a** piling of discrete pseudo-dodecamers; **b** continuous array of tetrameric disks covalently connected *via* the sugar phosphate groups. The disks represent the guanosine tetramers – schematically shown in **c** – while the grey circles indicate the sugar phosphodiesteric bridges. For simplicity, the helical arrangement along the rod axis is omitted

Table 1. SANS experimental results

Sample	C%	R_g(Å)	R_c(Å)	L(Å)	$d\Sigma/d\Omega(0)$ (cm^{-1})	$(d\Sigma/d\Omega(Q)Q)_{Q\to 0}$ (cm^{-1})
G1	1.0	–	–	–	–	–
G1	1.5	–	–	–	–	–
G2	1.0	21.4	9.9	69.2	0.021	9.1×10^{-4}
G2	1.5	23.3	10.5	71.2	0.037	16.4×10^{-4}
G3	1.0	20.1	10.1	62.1	0.019	9.3×10^{-4}
G3	1.5	20.9	9.1	69.1	0.034	14.6×10^{-4}
G4	1.0	20.4	9.6	62.9	0.019	9.1×10^{-4}
G6	1.0	19.3	10.1	59.7	0.021	10.7×10^{-4}
Uncertainty		±1.0	±1.0	±3.0	±0.003	$\pm2.0\times10^{-4}$

Linear behaviour was also observed in the low Q-range in the $\ln(d\Sigma/d\Omega(Q)Q)$ vs. Q^2 plot (see, as an example, that of the G3 derivative reported in the upper frame of Fig. 2), indicating that the scattering particles in solution have a cylindrical shape. We calculated the gyration radii of the cylinder cross section and the cross-sectional intensity for all samples at zero angle (Table 1). Noticeable is the fact that the different derivatives show an approximately constant cross-sectional gyration radius of about 10 Å, i.e. insensitive to the concentration and irrespective of the derivative considered. The length of the cylindrical particles was then estimated by using (7) and (8) and their mean values are reported in Table 1.

Discussion and structural interpretation

Previous structural studies showed that this series of guanosine derivatives form liquid crystalline mesophases (Spada et al. 1988; Mariani et al. 1989; Spada et al. 1991). In particular, it has been deduced that the cholesteric and hexagonal phases which exist between the isotropic and the crystalline states, consist of long chiral rod-shaped aggregates, whose sectional radius is about 12 Å. Each rod consists of a stacked array of planar tetramers, equally spaced at a distance of about 3.3 Å, and formed by Hoogsteen bonded guanosine moities (Mariani et al. 1989; Spada et al. 1991). Since our molecular unit is a short oligonucleoside phosphate, the rod structure can be attained with two possible and extreme models: piling of discrete barrels or a continuous array of cross-linked tetramers. As an example, we show in Fig. 3 the two ways in which G3 forms the rod aggregates: in the first, three adjacent tetrameric disks are connected by eight sugar-phosphate bridges to give a pseudo-dodecamer, while in the second, each tetrameric disk is covalently connected (*via* the sugar phosphate group) to the one above and to the one below, so that the rods show a continuous structure.

Apart from the case of G1 sample, which does not show any detectable signals in the investigated Q range,

the presence of the linear behaviour of the SANS data in the ln $((d\Sigma/d\Omega(Q))Q)$ vs. Q^2 plot (see, as an example, Fig. 2) suggests that the scattering particles have a cylindrical shape. As in the mesophase, guanosine derivatives also appear to be able to self-associate in order to form small rod-shaped aggregates in the isotropic phase (however, we must remember that D_2O, stabilizing the hydrophobic interactions, might favour such an aggregation process).

On the basis of this hypothesis, it is interesting to compare the observed gyration radii with the corresponding values $R_{g,mod}$ and $R_{c,mod}$ calculated from suitable models. Let us consider as a model a cylinder with radius R and height h. According to Kratky (1983), its gyration radius is defined by:

$$R_{g,mod} = ((2R^2 + h^2/3)/4)^{1/2}. \quad (9)$$

R and h are assumed according to previous X-ray diffraction results (Mariani et al. 1989; Spada et al. 1991) and to molecular dynamics calculations (Fisk et al. 1982). Since the X-ray diffraction analysis of the hexagonal phase showed that the sectional radius is quite insensitive to the sample concentration (Mariani et al. 1989; Spada et al. 1991), we considered the value determined at $C = 50\%$ (Mariani et al. 1989; Spada et al. 1991). Computer simulations (Fisk et al. 1982) showed that the coordination of the counterion to the phosphate may justify an increase of the tetrameric radius value up to 16 Å. Therefore, to overestimate the dimension of the model, we decided to consider 16 Å as a possible limit value. On the other hand, the rod-shaped structural elements which form the cholesteric and hexagonal phases are formed by stacked planar tetramers (Mariani et al. 1989; Spada et al. 1991). The stacking distance appeared fairly independent of the sample composition, therefore the height h of the cylindrical model can be related to the number n of stacked tetramers by using the following simple equation:

$$h = (n - 1)\Delta + 6.4 \quad (10)$$

where Δ is the distance between the piled disks, as determined in the hexagonal phase by X-ray diffraction experiments (Mariani et al. 1989; Spada et al. 1991) and the value 6.4 takes into account the hydration of the terminal disks (Fisk et al. 1982).

Once the geometrical parameters are selected, the comparison of the experimental data with the model is straightforward. The fitting procedure of the G3 derivative is shown in Fig. 4. The height h of the cylindrical aggregate and the corresponding radius of gyration $R_{g,mod}$ are reported as a function of the number of stacked disks for two values of the sectional radius (11.2 and 16 Å). Considering the experimental data, the best accord is found for $n = 18$ when $R = 11.2$ Å and for $n = 17$ when $R = 16$ Å, which correspond to a cylinder height h of 62.7 Å and of 59.4 Å, respectively. These results are summarized in table II, where we show the model structural parameters which give the best agreement with the experimental gyration radii R_g. Note that the lengths of the cylindrical aggregates found are consistent with those determined independently from the experimental SANS data ((7) and (8), see Table 1).

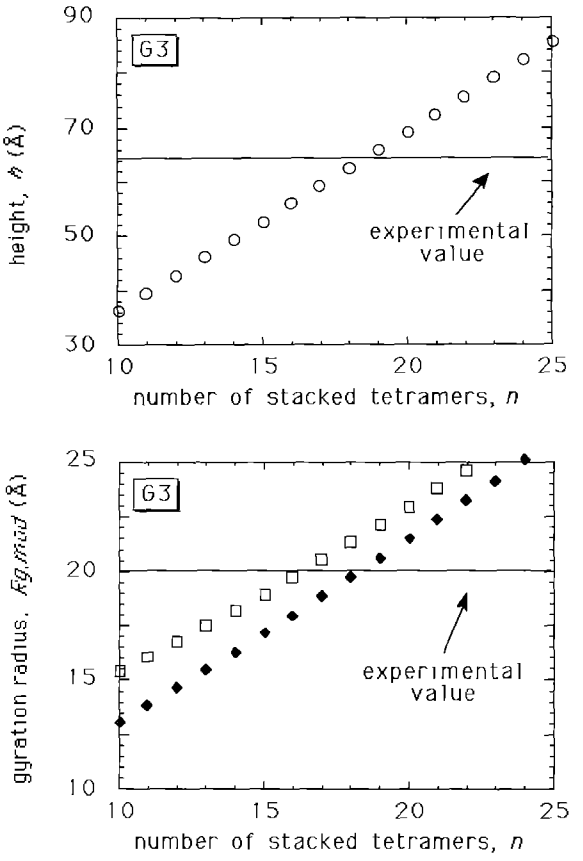

Fig. 4. Representative model fitting in the case of the G3 derivative ($C = 1\%$). Top diagram: height of the cylindrical model as a function of the number of piled disks. Bottom diagram: radius of gyration of the cylindrical model as a function of the number of piled disks; filled diamonds refer to a model radius of 11.2 Å (Spada et al. 1991) while open squares refer to a radius of 16 Å (Fisk et al. 1982). In both diagrams, a stright line indicates the value determined experimentally

A further confirmation of the validity of the proposed model is obtained by comparing the cross sectional gyration radii of the scattering particles observed for the different derivatives (see Table 1), with those calculated from (4) over a section of the model. As previously discussed, this section contains the tetramer Hoogsten-bonded guanosine residues (Saenger 1984; Mariani et al. 1989; Spada et al. 1991). Assuming a simplified representation in which the fluctations of atomic positions are neglected and the volumes of the different atoms are determined by averaging the whole molecular volume, we calculate an $R_{c,mod}$ of 10.3 Å, which is in very good agreement with the observed R_c (see Table 1).

Other instructive information could be obtained from the analysis of the scattered intensity at zero angle. By using (5), in fact, we can determine the number of scattering particles *per* unit volume. Because the mean particle composition can be directly derived from the model if the number n of stacked tetramers and the molecular formula of each derivative are considered, it is possible to calculate the number of molecules *per* unit volume which aggregate. These quantities, calculated assuming an H/D exchange parameter of 2.5 (Jacrot and Zaccai 1981), are shown in Table 3, where, for comparison, we also report

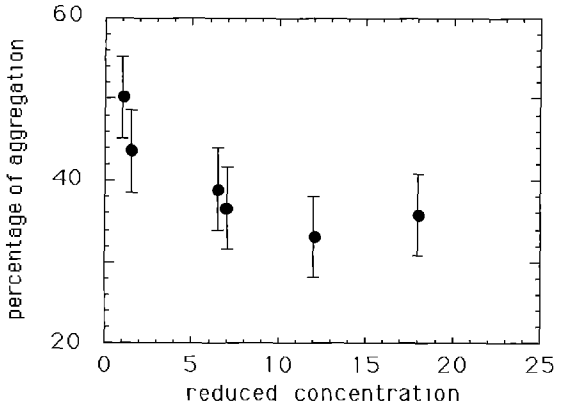

Fig. 5. Percentage of aggregation, as determined from the nominal concentration and the number of composition of scattering particles, as a function of the reduced concentration, i.e. the difference between the concentration corresponding to the isotropic to cholesteric phase transition and the one for the SANS measurements

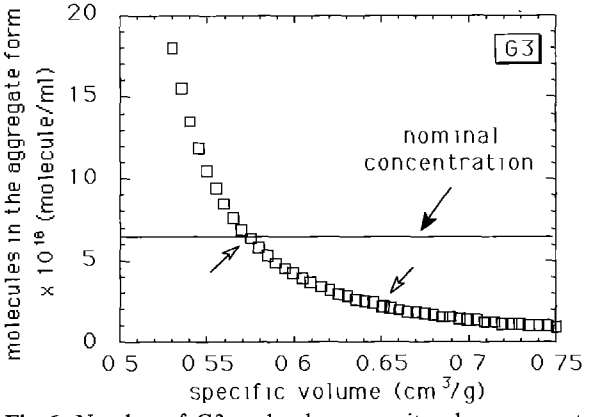

Fig. 6. Number of G3 molecules per unit volume present in the aggregate form in $C = 1\%$ solution as a function of the specific volume used to determine the scattering particle volume (see (2)). The right side open arrow marks the specific volume of 0.651 cm^3/g which has been used to calculate the data presented in Table 3. The left side open arrow indicates the specific volume of 0.57 cm^3/g, which corresponds to the full aggregation condition

Table 2. Structural model data

	G2	G3	G4	G6
$C = 1\%$				
Piled disk repeat distance, Δ (Å):	3.30	3.31	3.32	3.34
Cylinder radius,				
R (Å):	12.3 16.0	11.2 16.0	11.3 16.0	10.5 16.0
$R_{g,mod}$ (Å):	21.8 22.1	19.8 20.5	19.8 20.6	18.8 19.9
n	20 19	18 17	18 17	17 16
h (Å):	69.1 65.8	62.7 59 4	62.8 59.5	59.8 56.5
$C = 1.5\%$				
Piled disk repeat distance, Δ (Å):	3.30	3.31		
Cylinder radius,				
R (Å):	12.3 16.0	11.2 16.0		
$R_{g,mod}$ (Å):	22.6 22.9	21.5 22.2		
n	21 20	20 19		
h (Å):	72.4 69.1	69.3 66.0		

Table 3. Scattering intensity analysis

	G2	G3	G4	G6
$C = 1.0\%$				
N° of particles/cm^3 ($\times 10^{17}$)	1.10	1.00	0.89	0.99
Molecules *per* aggregate	40.1	23.8	18.0	11.3
Molecules/cm^3 in the aggregate from ($\times 10^{18}$)	4.41	2.38	1.59	1.13
Molecules/cm^3 in the "initial" solution ($\times 10^{18}$)	10.11	6.51	4.80	3.15
% of aggregation	43.6	36.6	33.1	35.8
$C = 1.5\%$				
N° of particles/cm^3 ($\times 10^{17}$)	1.84	1.43		
Molecules *per* aggregate	40.1	23.8		
Molecules/cm^3 in the aggregate from ($\times 10^{18}$)	7.60	3.81		
Molecules/cm^3 in the "initial" solution ($\times 10^{18}$)	15.16	9.77		
% of aggregation	50.2	39.0		

the nominal molecular concentration. A non-negligible discrepancy exists between the number of aggregate molecules and the nominal concentration, as emphasized by the calculated "percentage of aggregation". This means that only a fraction of molecules associate, while a second fraction remains in a true solution. Moreover, the comparison of results for experiments performed at different dilution indicates that a concentration-dependent equilibrium might exist. In fact, the percentage of aggregation changes, respectively, from about 43 to 50% and from about 37 to 39%, when the concentration of the G2 and G3 derivatives increases from 1 to 1.5%. This equilibrium seems to reflect the ability of different derivatives to form mesophases. In Fig. 5, the percentage of aggregation is plotted as a function of the *reduced concentration*, i. e. the difference between the concentration corresponding to the isotropic-to-cholesteric phase transition, as determined in normal water, and the one for the SANS measurements. It appears that the percentage of molecules which aggregate in solution decreases as long as the reduced concentration increases, i.e. as long as the nominal concentration is far from that of the isotropic-to-cholesteric phase transition. The experimental observation that G1 does not form any detectable aggregates confirms such a trend: in the series investigated G1 is the derivative which presents the highest reduced concentration and therefore the percentage of aggregation is expected to be rather low.

At present, however, other reasons could explain the discrepancy between the number of aggregate molecules and the nominal concentration. In particular, to determine the concentration of scattering particles, we must know their volume (see (5)). The results of this calculation appear to be very sensitive to the specific molecular vol-

ume. As an example, we show in Fig. 6 the case of the G3 derivative ($C = 1\%$), where the concentration of aggregated molecules was calculated as a function of the specific volume. In this figure, open arrows mark two particular values: the former is the specific volume which has been used to calculate the data presented in Table 3 (0.651 cm^3/g, as reported by Iball et al. (1963) for guanosine 5′-monophosphate; see also Mariani et al. 1989; Spada et al. 1991), while the second one indicates the specific volume (0.57 cm^3/g) which, according to the short cylindric model proposed above, corresponds to the full aggregation of G3 molecules. Such a value seems to be still reasonable, as it is consistent with the usually assumed DNA specific volume (0.55 cm^3/g; see for example Saenger 1984). Noticeable is the fact that this value does not significantly alter our previous structural analysis: for example, the radius of rods of the hexagonal phase at $C = 50\%$ changes, in the case of the G3 derivative, from 11.2 Å (Spada et al. 1991) to 10.7 Å, with a difference which is well inside the experimental error.

Conclusions

The main conclusion that can be derived from the present data is the fact that, excluding the case of the G1, the guanosine derivatives investigated retain the capacity of self-associate in the form of rod-shaped particles even in dilute solution. The SANS data indicated that these particles are roughly similar in the four different derivatives. On the basis of the structure of the neighbouring hexagonal and cholesteric phases (as determined by previous X-ray diffraction experiments), we fitted the experimental observations with a model of cylindrical aggregates formed by stacking about 18 to 20 Hoogsten-bonded guanosine tetramers. The calibration of the SANS intensities in absolute units allowed us the possibility to observe that two families of molecules exist in the isotropic phase, one in the aggregate form and the other in a "true" solution. An equilibrium seems to exist between these two molecular fractions, reflecting the ability of different derivatives to form mesophases: if the structural features of the aggregates are also considered, a common structural behaviour cannot be disregarded.

Acknowledgements. The samples were supplied by Dr. A. Garbesi and Dr. S Bonazzi (I. Co. C.E.A.–C.N.R., Ozzano Emilia, Italy), for which we are grateful. We are also indebted to Prof. F. Rustichelli, Prof. G. Gottarelli and Dr. G. P. Spada for helpful discussions. M. C. and P. M thank all people in Laboratoire Leon Brillouin (CEA-CEN Saclay, France), and in particular Dr. P. Calmettes, Dr. R. Giordano and Dr. J. Texeira, for experimental and instrumental support. M. C. and P. M. finally acknowledge the INFM (Italy) for financial support during their stay in Saclay. The work was supported by CNR, Regione Marche and MURST (Italy).

References

Abis S, Caciuffo R, Carsughi F, Coppola R, Magnani M, Rustichelli F, Stefanon M (1990) Late stages of δ' precipitation in an Al-Li alloy by small-angle neutron scattering. Phys Rev B42: 2275–2281

Chen SH, Lin TL (1987) Colloidal solutions. In: Celotta R, Levine J (eds) Methods in Experimental Physics, vol 23: Price DL, Skold K (eds) Neutron scattering, Part B, Academic Press, San Diego, pp 489–543

Fisk CL, Becker ED, Miles HT, Pinnavaia TJ (1982) Self-structured guanosine 5′-monophosphate. A ^{13}C and ^{1}H magnetic resonance study. J Am Chem Soc 104: 3307–3314

Gellert M, Lipsett MN, Davis DR (1962) Helix formation by guanylic acid. Proc Natl Acad Sci USA 48: 2013–2018

Guinier A, Fournet G (1955) Small angle scattering of X-rays. Wiley, New York

Hoogsten K (1959) Acta Crystallogr 12: 822–845

Iball J, Morgan CH, Wilson HR (1963) Fibres of guanine nucleosides and nucleotides. Nature 199: 688–689

Jacrot B (1976) The study of biological structures by neutron scattering from solution. Rep Prog Phys 39: 911–953

Jacrot B, Zaccai G (1981) Determination of molecular weight by neutron scattering. Biopolymers 20: 2413–2426

Jin R, Breslauer KJ, Jones RA, Gaffney BL (1990) Tetraplex formation of a guanine-containing nonameric DNA fragment. Science 250: 543–546

Kratky O (1983) Diffuse small-angle scattering of macromolecules in solution. In: Hoppe W, Lohmann HM, Ziegler H (eds) Biophysics. Springer, Berlin Heidelberg New York, pp 65–74

Kratky O, Laggner P (1987) X-ray small-angle scattering. Encyclopedia Phys Sci Technol 14: 693–742

Mariani P, Mazabard C, Garbesi A, Spada GP (1989) A study of the structure of the lyomesophases formed by the dinucleoside phosphate d(GpG). An approach by X-ray diffraction and optical microscopy. J Am Chem Soc 111: 6369–6373

Perkins SJ, Chung P, Reid KBM (1986) Unusual ultrastructure of complement-component-C4b-binding protein of human complement by synchrotron X-ray scattering and hydrodynamic analysis. Biochem J 233: 799–807

Saenger W (1984) Principles of nucleic acid structure, Springer, New York Berlin Heidelberg, pp 315–320

Spada GP, Carcuro A, Colonna FP, Garbesi A, Gottarelli G (1988) Lyomesophases formed by the dinucleoside phosphate d(GpG). Liquid Crystals 3: 651–654

Spada GP, Mariani P, Gottarelli G, Garbesi A, Bonazzi S, Ponzi Bossi MG, De Morais MM, Capobianco M (1991) Four-stranded aggregates of oligodeoxyguanylates forming lyotropic liquid crystals: a study by circular dichroism, optical microscopy and X-ray diffraction. J Am Chem Soc 113: 5809–5816

Sundquist WI, Klug A (1989) Telomeric DNA dimerizes by formation of guanine tetrads between hairpin loops. Nature 342: 825–829

Zimmerman SB (1976) X-ray study by fiber diffraction methods of a self-aggregate of guanosine-5′-phosphate with the same helical parameters as Poly(rG). J Mol Biol 106: 663–672